The odorant receptor OR2W3 on airway smooth muscle evokes bronchodilation via a cooperative chemosensory tradeoff between TMEM16A and CFTR

Jessie Huang[a,1,2], Hong Lam[a,1], Cynthia Koziol-White[b,c], Nathachit Limjunyawong[d], Donghwa Kim[e], Nicholas Kim[b], Nikhil Karmacharya[c], Premraj Rajkumar[f], Danielle Firer[a], Nicholas M. Dalesio[g], Joseph Jude[c], Richard C. Kurten[h], Jennifer L. Pluznick[f], Deepak A. Deshpande[i], Raymond B. Penn[i], Stephen B. Liggett[e,j], Reynold A. Panettieri Jr[c], Xinzhong Dong[d,k], and Steven S. An[b,c,2]

[a]Department of Environmental Health and Engineering, The Johns Hopkins University Bloomberg School of Public Health, Baltimore, MD 21205; [b]Department of Pharmacology, Rutgers-Robert Wood Johnson Medical School, The State University of New Jersey, Piscataway, NJ 08854; [c]Rutgers Institute for Translational Medicine and Science, New Brunswick, NJ 08901; [d]Solomon H. Snyder Department of Neuroscience, The Johns Hopkins University School of Medicine, Baltimore, MD 21205; [e]Center for Personalized Medicine, Morsani College of Medicine, University of South Florida, Tampa, FL 33612; [f]Department of Physiology, The Johns Hopkins University School of Medicine, Baltimore, MD 21205; [g]Department of Anesthesiology and Critical Care Medicine, The Johns Hopkins University School of Medicine, Baltimore, MD 21205; [h]Department of Physiology and Biophysics, University of Arkansas for Medical Sciences, Little Rock, AR 72205; [i]Division of Pulmonary and Critical Care Medicine, Department of Medicine, Center for Translational Medicine, Jane and Leonard Korman Respiratory Institute, Thomas Jefferson University, Philadelphia, PA 19107; [j]Department of Medical Engineering, University of South Florida, Tampa, FL 33612; and [k]Howard Hughes Medical Institute, The Johns Hopkins University School of Medicine, Baltimore, MD 21205

Edited by Mark T. Nelson, University of Vermont, Burlington, VT, and approved September 22, 2020 (received for review February 18, 2020)

The recent discovery of sensory (tastant and odorant) G protein-coupled receptors on the smooth muscle of human bronchi suggests unappreciated therapeutic targets in the management of obstructive lung diseases. Here we have characterized the effects of a wide range of volatile odorants on the contractile state of airway smooth muscle (ASM) and uncovered a complex mechanism of odorant-evoked signaling properties that regulate excitation-contraction (E-C) coupling in human ASM cells. Initial studies established multiple odorous molecules capable of increasing intracellular calcium ($[Ca^{2+}]_i$) in ASM cells, some of which were (paradoxically) associated with ASM relaxation. Subsequent studies showed a terpenoid molecule (nerol)-stimulated OR2W3 caused increases in $[Ca^{2+}]_i$ and relaxation of ASM cells. Of note, OR2W3-evoked $[Ca^{2+}]_i$ mobilization and ASM relaxation required Ca^{2+} flux through the store-operated calcium entry (SOCE) pathway and accompanied plasma membrane depolarization. This chemosensory odorant receptor response was not mediated by adenylyl cyclase (AC)/cyclic nucleotide-gated (CNG) channels or by protein kinase A (PKA) activity. Instead, ASM olfactory responses to the monoterpene nerol were predominated by the activity of Ca^{2+}-activated chloride channels (TMEM16A), including the cystic fibrosis transmembrane conductance regulator (CFTR) expressed on endo(sarco)plasmic reticulum. These findings demonstrate compartmentalization of Ca^{2+} signals dictates the odorant receptor OR2W3-induced ASM relaxation and identify a previously unrecognized E-C coupling mechanism that could be exploited in the development of therapeutics to treat obstructive lung diseases.

olfactory receptor | G proteins | airway smooth muscle | single-cell analysis | asthma

Asthma, an inflammatory disorder of airways, presents a global healthcare challenge with over 300 million individuals now afflicted worldwide (1). The root cause of asthma morbidity, and in some cases death, is airway hyperresponsiveness (AHR) or excessive airway narrowing due to airway smooth muscle (ASM) shortening (2–4). An enhanced shortening of ASM cells contributes to asthma exacerbations from a variety of stimuli such as exercise, cold air, allergens, air pollution, and viral infection (5–8).

β-Agonists are effective bronchodilators, routinely utilized for the acute treatment of bronchospasm and for the prophylactic management of asthma symptoms when chronically administered. These agents relieve airflow obstruction by activating β_2-adrenergic receptors (β_2ARs) that are G protein-coupled receptors (GPCRs) expressed on the smooth muscle of human bronchi, inhibiting basal tone and ASM shortening (9, 10). The regular use of β-agonists, however, can induce drug tolerance or loss of their clinical efficacy (11). In addition, increased airway inflammation (12), bronchial hyperreactivity (13, 14), and other adverse effects, including death (15, 16), have been observed in various clinical trials of β-agonists. Consequently, there is an unmet need to identify new therapeutic targets whose activation or inhibition can directly modulate excitation-contraction (E-C) coupling and relax ASM.

We have recently reported "sensory" GPCRs of the bitter taste receptor (TAS2R) family and the olfactory receptor (OR)

Significance

Odorant sensing GPCRs are the largest gene family in the human genome. We previously found multiple olfactory receptors and their obligate downstream effectors expressed in the smooth muscle of human bronchi. However, the extent to which odorant-sensing receptors (and the ligands to which they respond) on airway smooth muscle (ASM) are physiologically relevant is not established. Here we show that a monoterpene nerol activates the odorant receptor OR2W3 to relax ASM in both cell and tissue models. Surprisingly, the mechanism of action of OR2W3-mediated ASM relaxation involves paradoxical increases in $[Ca^{2+}]_i$ that invoke a cooperative activation of TMEM16A and CFTR to compartmentalize calcium and regulate excitation-contraction coupling in human ASM cells.

Author contributions: J.H., H.L., J.L.P., and S.S.A. designed research; J.H., H.L., C.K.-W., N.L., D.K., N. Kim, N. Karmacharya, D.F., and J.J. performed research; C.K.-W., P.R., N.M.D., J.J., R.C.K., J.L.P., D.A.D., R.B.P., S.B.L., R.A.P., X.D., and S.S.A. contributed new reagents/analytic tools; J.H., H.L., C.K.-W., N.L., D.K., N. Kim, N. Karmacharya, D.A.D., R.B.P., S.B.L., R.A.P., X.D., and S.S.A. analyzed data; J.H. and S.S.A. wrote the paper; and S.S.A. directed all studies.

The authors declare no competing interest.

This article is a PNAS Direct Submission.

[1]J.H. and H.L. contributed equally to this work.

[2]To whom correspondence may be addressed. Email: hjess@bu.edu or sa1510@rbhs.rutgers.edu.

This article contains supporting information online at https://www.pnas.org/lookup/suppl/doi:10.1073/pnas.2003111117/-/DCSupplemental.

First published October 23, 2020.

family expressed on human ASM cells (17–19). TAS2Rs reverse bronchoconstriction by an unclear mechanism that is associated with Ca^{2+}-activated K^+ (BK_{Ca}) channels, evoking membrane hyperpolarization and ASM relaxation (19–22). Human ASM cells also express multiple ORs and their obligate downstream effectors, the olfactory G protein (G_{olf}) and adenylyl cyclase III (AC3) (17). Of note, activation of the odorant receptor OR51E2 via its cognate ligands acetate and propionate results in marked reductions in cytoskeletal remodeling and ASM proliferation (17). These physiological outcomes mediated by endogenous metabolic byproducts of the gut microbiota (i.e., short chain fatty acids) suggest previously unidentified "ancient" chemosensors of the gut-lung axis. The findings also give rise to the notion that ectopic expressions of sensory receptors can be exploited to discover disease-modifying therapeutics for asthma (23).

Here we tested on ASM the physiological effects of volatile chemicals occupying a wide odorant space, using optical magnetic twisting cytometry (OMTC). After having established both procontractile and prorelaxant effects of various odorous molecules, subsequent studies focused on the regulatory mechanism of a terpenoid odorant (nerol) on ASM signaling and shortening through its reported odorant receptor OR2W3 (24–26). The monoterpene nerol evoked calcium flux, relaxed isolated human ASM cells in vitro, and reversed carbachol-induced bronchoconstriction ex vivo in human precision cut lung slices (hPCLSs). Down-regulation of OR2W3 in human ASM cells by RNA interference led to significant inhibitions of nerol-induced $[Ca^{2+}]_i$ mobilization and ASM relaxation. Surprisingly, OR2W3-mediated increases in $[Ca^{2+}]_i$ and the associated ASM relaxation were narrowly tuned to the store-operated calcium entry (SOCE) pathway and accompanied membrane depolarization, displaying signaling properties distinct from those of the β_2AR and TAS2R. The chemosensory mechanism of the odorant receptor OR2W3 in ASM did not involve adenylyl cyclase (AC)/cyclic nucleotide-gated (CNG) channels, but was predominated by the activity of Ca^{2+}-activated chloride channels belonging to the anoctamine family of membrane proteins (TMEM16A) and the cystic fibrosis transmembrane conductance regulator (CFTR) expressed on endo(sarco)plasmic reticulum (ER). These findings further advance the fledgling concept that compartmentalization dictates the multifaceted effects of $[Ca^{2+}]_i$ on ASM contractile state.

Results and Discussion

Volatile Odorants Evoke Calcium Flux in Human ASM Cells. Odorant-sensing GPCRs are the largest gene family in the human genome (27) and are expressed on the smooth muscle of human bronchi (17). The functional and physiological roles of olfactory receptors expressed on ASM, and the ligands to which they respond, are unestablished.

Using isolated human ASM cells, we characterized the direct effects of 20 volatile chemicals comprised of ketones, aldehydes, amines, alkenes, and alcohols (*SI Appendix*, Table S1), representing seven discrete odor types (i.e., putrid, nutty, fruity, floral, caramellic, herbaceous, and minty). Because sensory transduction in the main olfactory epithelium primarily involves opening of CNG, nonselective cation channels, and the consequent influx of Ca^{2+} (27–29), we first assessed in ASM cells the signaling properties of each odorous molecule. We used the FLIPR Calcium 5 assay to measure $[Ca^{2+}]_i$ and used a conventional, colorimetric cAMP ELISA to measure $[cAMP]_i$.

In this space of odorants tested, eight odorants evoked a rapid rise in $[Ca^{2+}]_i$ (Fig. 1*A*). The $[Ca^{2+}]_i$ transients elicited by these odorant subsets (e.g., citralva, β-ionone, hedione, lilial, nerol, geraniol, eugenol, and ethyl vanillin) were similar to those stimulated by histamine, an agent which causes ASM contraction (Fig. 1*A* and *SI Appendix*, Fig. S1*A*). In contrast, compared to vehicle control (0.1% dimethyl sulfoxide [DMSO]), we found that two odorants tetramethylpyrazine and hedione appreciably increased $[cAMP]_i$ in human ASM cells (*SI Appendix*, Fig. S1*B*, ANOVA with Dunnet's method, $n = 4$ to 6 independent samples). The magnitude of tetramethylpyrazine- and hedione-induced $[cAMP]_i$ was similar to that elicited by the (prorelaxant) β-agonist isoproterenol.

Volatile Odorants Have Diverse Effects on ASM Contractility. Using OMTC, we next measured dynamic changes in cell stiffness in response to volatile odorants, as an index of single-cell contractility (7). Similar to the mechanical responses to histamine and isoproterenol (i.e., contraction and relaxation) (7, 19), most of the odorants (17/20) caused stiffness changes in individual ASM cells (Fig. 1*B*). As shown in Fig. 1*B*, odorants occupying the space of putrid smell (isovaleric acid, triethylamine, and pyrrolidine) markedly increased the stiffness of isolated human ASM cells; the magnitude of cell stiffening was similar to that elicited by histamine (*SI Appendix*, Fig. S1*C*). Conversely, odorants spanning six nonmalodor types (i.e., nutty, fruity, floral, caramellic, herbaceous, and minty smells) decreased the cell stiffness, similar to the effect of the β-agonist isoproterenol (Fig. 1*B* and *SI Appendix*, Fig. S1*C*). Strikingly, and contrary to histamine-induced $[Ca^{2+}]_i$ associated with ASM contraction, nonmalodorous scents capable of increasing $[Ca^{2+}]_i$ caused the relaxation of ASM cells (Fig. 1 and *SI Appendix*, Fig. S1). Together these results established that the smooth muscle of human bronchi has the capacity to chemically sense a wide range of odorants with differing abilities to regulate bronchomotor tone and ASM shortening.

In this space of nonmalodorous chemicals, a class of terpenoid molecules (nerol, citronellol, eugenol, and linalool) are reported ligands for various human and mouse olfactory receptors (26, 30–32). The monoterpene nerol, for example, is a cognate ligand for the odorant receptor OR2W3 in human spermatozoa, and elicits $[Ca^{2+}]_i$ and sperm chemotaxis (24–26). Because terpenoid molecules are known to possess antimicrobial, antiinflammatory, and antispasmodic properties (33–36) that may serve therapeutic functions in the management of obstructive lung diseases, we focused herein on the physiological effects of the odorant nerol and its mechanism of action through OR2W3 expressed on human ASM cells.

The Monoterpene Nerol Evokes Calcium Signaling, Causes ASM Relaxation, and Reverses Obstruction. In isolated human ASM cells, the monoterpene nerol increased $[Ca^{2+}]_i$ (Fig. 2*A*) and caused ASM relaxation (Fig. 2*B*) in a dose-dependent manner, with half maximal effective concentrations (EC_{50}) of ~526 μM and ~574 μM, respectively. The nerol EC_{50} values for $[Ca^{2+}]_i$ and ASM relaxation suggest a causal relationship between nerol-evoked calcium signaling and ASM relaxation. In hPCLSs, nerol (>500 μM) reversed carbachol-induced bronchoconstriction with the patency of small airways equivalent to basal conditions (prior to carbachol stimulation) (Fig. 2*C*). Fig. 2*D* showed the expected between-lung and between-donor variations in nerol-induced bronchodilation (12 lung slices derived from three different nonasthmatic lung donors). Mixed effect analysis revealed significant bronchodilatory responses to nerol at 1 mM and 3 mM, resulting in ~18.8 ± 7.6% and 47.0 ± 9.8% increase in the luminal area from carbachol-constricted airways, respectively (Fig. 2*D*). These results suggested that the monoterpene nerol can bronchodilate and reverse airflow obstruction via its prorelaxant effects on ASM, involving calcium signaling.

Of note, exposure to nerol (500 to 1,000 μM), at both short and long time scales, did not induce cAMP generation in human ASM cells (*SI Appendix*, Fig. S2*A*). Moreover, nerol-induced ASM relaxation was unaffected in cells treated with pharmacological inhibitors of adenylyl cyclase (SQ22536, 100 μM) and protein kinase A (H89, 10 μM) (*SI Appendix*, Fig. S2*B*); cells

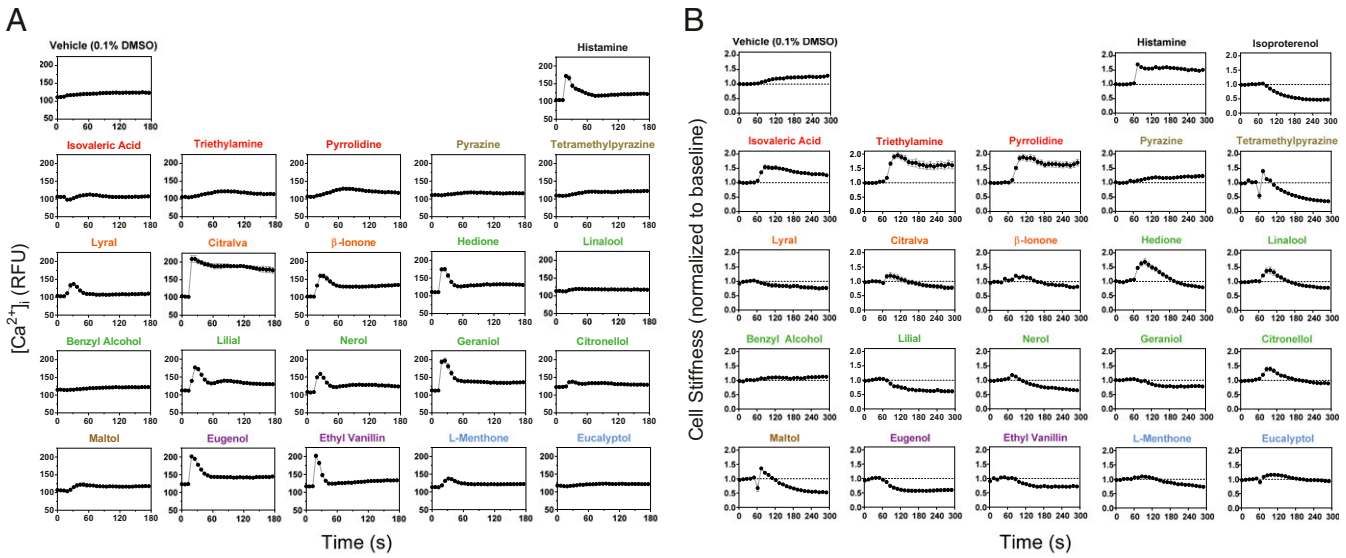

Fig. 1. Intracellular calcium flux and single-cell contractility evoked by 20 volatile odorants. (*A*) Odorant-evoked $[Ca^{2+}]_i$ was measured using FLIPR Calcium 5 assay. For each well of human ASM cells (~30,000 cells/well), baseline Calcium 5 dye fluorescence was measured for the first 15 s, and after odorant addition (t = 15 s), the fluorescent reading was continuously measured using a FlexStation 3. For vehicle control, $[Ca^{2+}]_i$ was measured in response to 0.1% DMSO. As positive control, cells were stimulated with 10 μM histamine. Data are presented as mean ± SE ($n = 3$ independent measurements). (*B*) Dynamic changes in the stiffness of human ASM cells were measured in response to each odorant molecule using OMTC. For each individual human ASM cell, baseline stiffness was measured for the first 60 s, and after odorant addition (t = 60 s), stiffness was continuously measured for the next 240 s. For each cell, stiffness was normalized to its baseline stiffness prior to odorant stimulation (normalized baseline is indicated by dotted line). For vehicle control, stiffness was measured in response to 0.1% DMSO. As positive controls, cell were contracted with 10 μM histamine and relaxed with 10 μM isoproterenol. Data are presented as mean ± SE ($n = 92$ to 403 individual cell measurements). The colors indicated the odor types of 20 volatile chemicals (putrid, nutty, fruity, floral, caramellic, herbaceous, and minty); the concentrations used for each odorant molecule are shown in *SI Appendix*, Table S1.

treated with H89 exhibited significant ($P < 0.001$) increases in baseline cell stiffness, suggesting the regulation of basal tone by protein kinase A (PKA) (37). In addition, costimulation with nerol and isoproterenol (β-agonist), both at submaximal doses, induced ASM relaxation that was greater than that with either compound alone (*SI Appendix*, Fig. S2 *C* and *D*). These data showed that nerol-induced ASM relaxation is additive with β-agonists, is not mediated by G_s signaling, and is independent of PKA activity.

Nerol-Induced ASM Relaxation Is Not Mediated via TRP Channels. A number of studies have reported that monoterpenes can act upon the transient receptor potential (TRP) family of nonselective cation channels, i.e., as agonist for TRPV1 (transient receptor potential vanilloid 1) and agonist/antagonist for TRPM8 (transient receptor potential melastatin 8) (38–40). In our OMTC studies, we found that TRPM8 agonist menthol, including TRPA1 [ankyrin (A) TRP channel] agonist allyl isothiocyanate (AITC), markedly decreased the cell stiffness, but not TRPV1 agonist capsaicin (*SI Appendix*, Fig. S3, as ascertained by one-sample *t* test). Compared with vehicle control (0.1% DMSO), the stiffness decrease in response to menthol was evident within 10 s ($P < 0.001$ at t = 70 s) while evident within 29 s ($P < 0.005$ at t = 88.7 s) for AITC (ANOVA at each time). None of the pharmacological antagonists decreased the cell stiffness (*SI Appendix*, Fig. S3).

Of note, preexposing human ASM cells for 10 min with either TRPM8 antagonist BCTC, TRPA1 antagonist HC-030031, or TRPV1 antagonist capsazepine had little effects on nerol-induced calcium signaling (Fig. 3*A*) and stiffness decreases (Fig. 3*B*). Although we cannot rule out a possible role of other TRP channels, these results suggested that nerol-induced ASM relaxation does not invoke ligand-gated extracellular Ca^{2+} influx and/or Ca^{2+} release through classical "pain"-, "temperature"-, and "itch"-sensitive TRP channels (i.e., TRPV1, TRPM8, and TRPA1). Based on these findings, we next assessed the mechanism of action of the monoterpene nerol through its reported odorant receptor OR2W3.

OR2W3 Is a Discriminatory GPCR Sensor for Terpenoid Odorants. OR2W3 is one of the most highly abundant odorant-sensing GPCR transcripts mapped to the human ASM olfactome (17). We confirmed the presence of OR2W3 at the mRNA and protein levels in human ASM cells. As shown in Fig. 4*A*, we detected the full-length OR2W3 mRNA at the expected 945 bp using PCR; the PCR product was sequenced to confirm its identity. Using qRT-PCR and Western blots, we validated the mRNA and protein expressions of OR2W3 in ASM cells derived from three different nonasthmatic lung donors (Fig. 4 *B* and *C*). The specificity and sensitivity of primary antibodies used against OR2W3 are shown in *SI Appendix*, Fig. S4. Using immunohistochemistry, we also detected the expression of OR2W3 in human ASM cells (*SI Appendix*, Fig. S4 *C* and *D*). Of note, we found that the transcript levels of OR2W3, as well as the extent of ASM relaxation in response to nerol, were not significantly different in cells derived from nonasthmatic ($n = 6$) vs. asthmatic ($n = 6$) lung donors (Fig. 4 *D* and *E*).

In order to show that nerol-evoked ASM signaling and function are mediated through the odorant receptor OR2W3, we next performed loss-of-function studies using short-hairpin (sh) RNAs targeting OR2W3. As shown in Fig. 5*A*, shRNAs complementary to OR2W3 mRNAs decreased OR2W3 transcripts in human ASM cells (65 ± 3.0% reduction in shOR2W3-1 and 53 ± 6.0% in shOR2W3-2). The transcripts for other highly enriched ASM ORs (e.g., OR1J1 and OR6A2) (17), including β_2-adrenergic receptor (ADRB2), were unaffected in shOR2W3-1 and shOR2W3-2 clones (Fig. 5*A*). Under these levels of OR2W3 down-regulation, the magnitude of nerol-induced

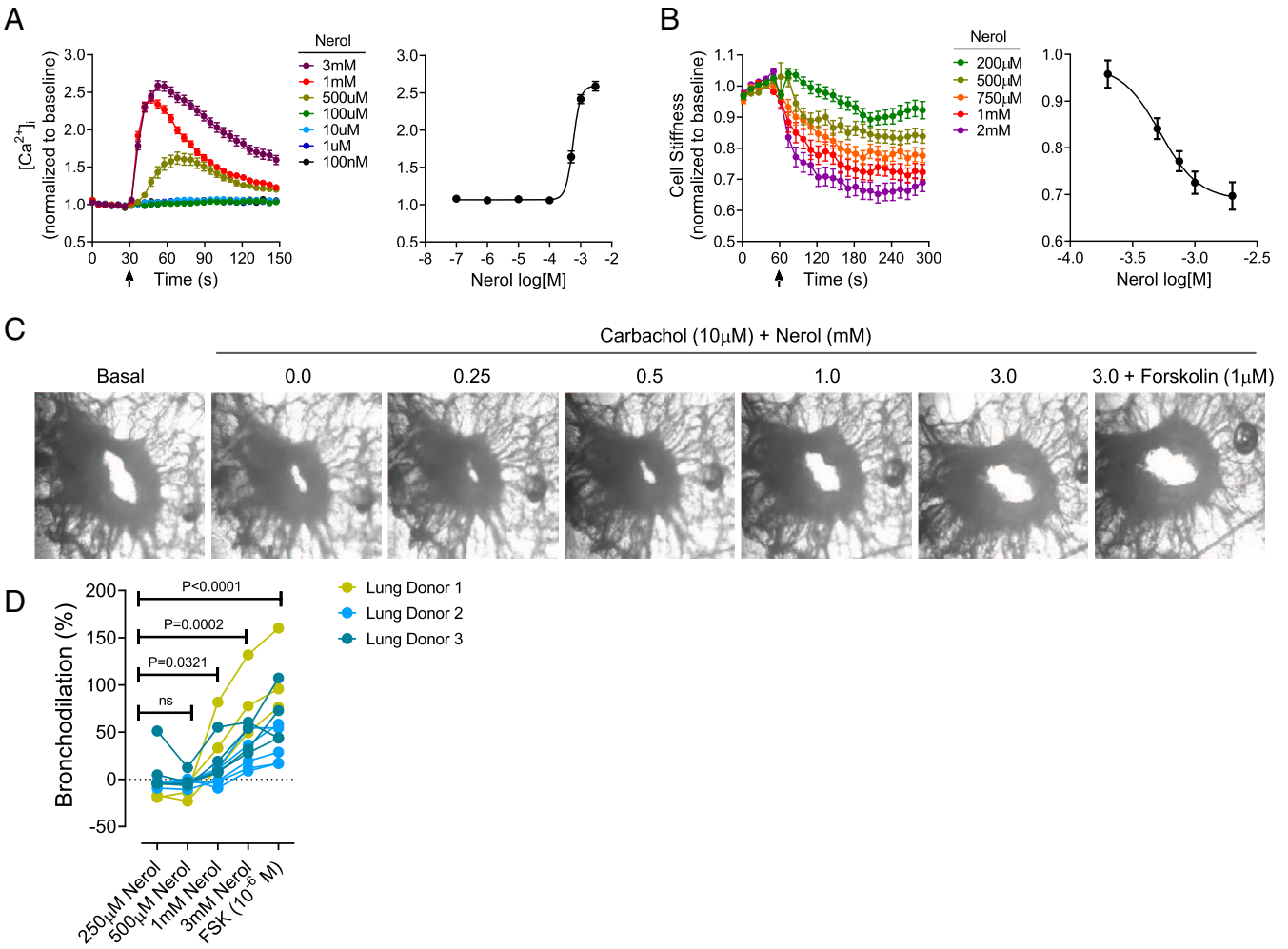

Fig. 2. Nerol evokes calcium flux, ASM relaxation, and bronchodilation. (*A*) Nerol-evoked $[Ca^{2+}]_i$ and EC_{50} of $[Ca^{2+}]_i$ response in isolated human ASM cells. Data are presented as mean ± SE (n = 90 to 123 cells per group). (*B*) Nerol-induced stiffness changes and EC_{50} of stiffness response. Data are presented as mean ± SE (n = 124 to 219 individual cell measurements). (*C*) Representative images of small airways before and after constricted with 10 μM carbachol (for 10 min), followed by stimulation with increasing doses of nerol (5 min for each dose). After nerol exposures, lung slices were relaxed with forskolin (1 μM) as positive control. (*D*) Individual hPCLS responses to increasing doses of nerol. Nerol-induced bronchodilation was measured in a total of 12 hPCLSs derived from three different nonasthmatic lung donors. To control for random effects from multiple lung slices from the same donor, we applied a linear mixed effect model using SAS V.9.2 (SAS Institute). ns, not significant.

calcium signaling displayed a varied effect at below EC_{50} values (e.g., 125 to 250 μM). Both shOR2W3-1 and shOR2W3-2, however, showed appreciable attenuations in nerol-induced $[Ca^{2+}]_i$ (peak) and ASM relaxation compared to that of scramble shRNA control (Fig. 5 *B* and *C*). Of note, in both clones, ASM relaxation responses to nerol were markedly attenuated in all concentrations of nerol tested, except 1 mM (*SI Appendix*, Fig. S5*C*). These results suggested that, in human ASM cells, the physiological responses to the monoterpene nerol are tranduced in part by the activation of its reported odorant-sensing OR2W3 (26).

To further characterize the potential receptor-ligand interactions of the odorant receptor OR2W3 with its reported ligand nerol, we also applied a recently described method called DREAM (deorphanization of receptors based on expression alterations in mRNA levels) (41, 42). This method identifies the cognate receptor-ligand pairs through dynamic alterations of the receptor transcripts (42). Human ASM cells exposed to nerol showed decreases in OR2W3 transcripts that were dose and time dependent, with the maximal effects at 1 mM and at 24 h (*SI Appendix*, Fig. S5 *A* and *B*). Nerol exposure had little effect on the transcript levels of OR1J1 and OR6A2 (*SI Appendix*, Fig. S5 *B* and *C*). Interestingly, the monocyclic monoterpene eugenol also decreased OR2W3 transcripts in human ASM cells, whereas monoterpenoids L-menthone (monoterpene ketone) and eucalyptol (monoterpene oxide) did not (*SI Appendix*, Fig. S5*C*). In addition, human ASM cells exposed to geraniol (a geometric isomer of nerol) and citronellol (dihydrogeraniol) showed marked reductions in OR2W3 mRNAs, but not to linalool (a structural isomer of nerol/geraniol). Together these data provided further support that OR2W3 expressed on human ASM cells is a monoterpene-activated olfactory GPCR.

OR2W3-Evoked Ca^{2+} Flux Is Functionally Divergent from That of TAS2Rs. In human ASM cells, TAS2Rs signal to phospholipase C (PLCβ) and produce a localized Ca^{2+} release, membrane hyperpolarization, and smooth muscle relaxation partially through large conductance BK_{Ca} channels (19, 20). Accordingly, we examined whether OR2W3-induced ASM relaxation may also involve a compartmentalized Ca^{2+} signal.

To this end, we employed selective pharmacological inhibitors of TAS2R signaling intermediates (gallein for $G_{\beta\gamma}$ and U73122

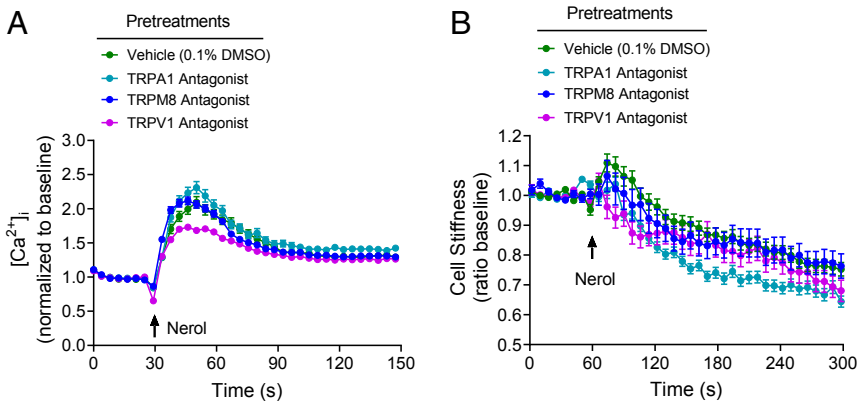

Fig. 3. The role for classical pain-, temperature-, and itch-sensitive TRP channels on nerol-induced ASM responses. Human ASM cells were treated for 10 min with 5 μM BCTC, 30 μM HC-030031, or 5 μM capsazepine, and then stimulated with 1 mM nerol. For vehicle control, cells were treated for 10 min with 0.1% DMSO. Nerol-induced $[Ca^{2+}]_i$ (*A*) and stiffness changes (*B*) were measured using Fura-2 and OMTC, respectively. Data are presented as mean ± SE (*A*, $n = 94$ to 153 individual cell measurements; *B*, $n = 140$ to 281 individual cell measurements). Arrows indicated the time at which nerol was added.

for PLCβ), including iberiotoxin and charybdotoxin for BK_{Ca} channels (19, 20). In addition, we measured nerol-induced ASM relaxation under experimental conditions in which internal stores were depleted of calcium with thapsigargin (19, 43). Nerol-induced ASM relaxation was not inhibited by pharmacological inhibitions of $G_{\beta\gamma}$, PLCβ, and BK_{Ca} channels (Fig. 6*A*), nor depleting intracellular calcium stores with thapsigargin (Fig. 6*B*). While U73122 treatment had little effect on the cell stiffness or nerol-induced stiffness decreases (Fig. 6*A*), it markedly reduced $[Ca^{2+}]_i$ transients evoked by nerol (*SI Appendix*, Fig. S6*A*). These findings suggest that OR2W3-evoked calcium release through PLCβ is necessary, but not sufficient to cause ASM relaxation.

Interestingly, nerol-stimulated increases in $[Ca^{2+}]_i$ and the associated relaxation of ASM cells were completely inhibited by chelating extracellular calcium with ethylene glycol-bis(β-aminoethyl ether)-*N*,*N*,*N*′,*N*′-tetraacetic acid (EGTA) (Fig. 6*B* and *SI Appendix*, Fig. S6*B*); depleting intracellular calcium stores had little effects. As expected, depleting intracellular stores markedly inhibited $[Ca^{2+}]_i$ transients and ASM contraction induced by G_q-coupled receptor agonist histamine (Fig. 6*B* and *SI Appendix*, Fig. S6*B*). These results showed that OR2W3-dependent ASM responses require extracellular Ca^{2+} influx, suggesting a mechanism distinct from Ca^{2+} signal tranduced by TAS2Rs. Consistent with this notion, costimulation with submaximal doses of nerol and chloroquine (TAS2R agonist) showed enhanced relaxation responses relative to that caused by stimulation with either compound alone (*SI Appendix*, Fig. S6*C*).

Chemosensory OR2W3 Responses Are Associated with Depolarization of the Cell Membrane. Contrary to the regulation of E-C coupling in smooth muscle by other prorelaxant agents (19, 44, 45), nerol-mediated ASM relaxation was accompanied by depolarization of

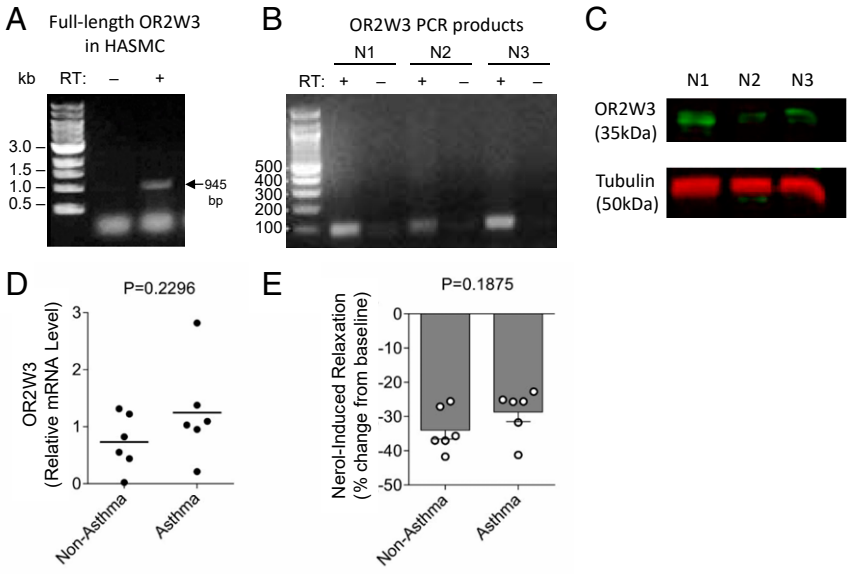

Fig. 4. Human ASM cells express OR2W3. (*A*) Expression of OR2W3 transcripts in human ASM cells was detected using PCR with (+) or without (–) reverse transcriptase. Full-length OR2W3 is indicated at 945 bp. (*B*) PCR was also applied to RNAs isolated from cells derived from three additional nonasthmatic lung donors (N1 to N3); PCR products were subsequently run on an agarose gel with or without reverse transcriptase. (*C*) Protein expression of OR2W3 (35 kDa) was assessed by Western blot in human ASM cells derived from three nonasthmatic lung donors (N1 to N3). Tubulin (50 kDa) was used as loading control. (*D*) Transcript levels of OR2W3 and (*E*) nerol-induced ASM relaxation in cells derived from six nonasthmatic and six asthmatic lung donors. Group mean of nerol-induced ASM relaxation is presented as percent change from the respective baseline stiffness.

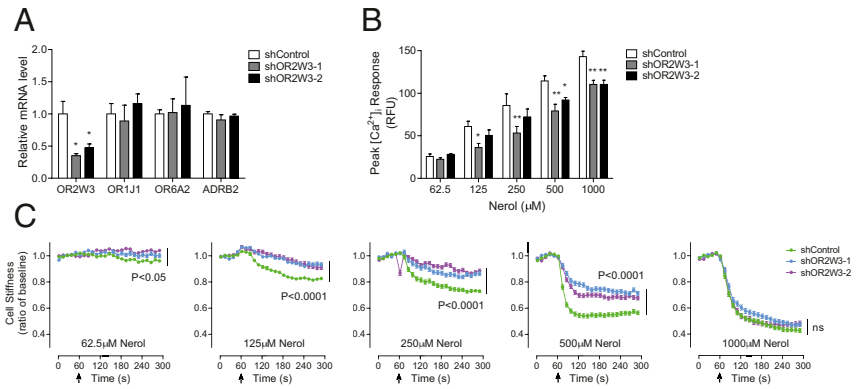

Fig. 5. OR2W3-evoked calcium flux causes ASM relaxation. (*A*) Short hairpin RNAs complementary to OR2W3 mRNAs markedly knockdown OR2W3, but not other ORs and β_2-adrenergic receptor (ADRB2) in human ASM cells. Data are presented as mean ± SE (n = 3 independent measurements). We used Kruskal–Wallis test and applied Dunn's method for multiple comparisons. P values indicate the statistical differences from shControl. (*B*) Peak $[Ca^{2+}]_i$ and (*C*) stiffness changes to nerol in shOR2W3 vs. shControl cells. Data are presented as mean ± SE (control shRNA, n = 282 to 377; OR2W3 shRNA #1, n = 266 to 368; OR2W3 shRNA #2, n = 210 to 345 individual cell measurements). (*B* and *C*) We used ANOVA with adjusting for multiple comparisons by applying the Dunnet's method. P values indicate the statistical differences from shControl. $*P < 0.05$, $**P < 0.01$.

the cell membrane (Fig. 6*C*). As expected, the bitter tastant chloroquine caused membrane hyperpolarization while the contractile agonist histamine caused membrane depolarization in human ASM cells (Fig. 6*D*). Nerol-induced plasma membrane depolarization was not due to cell injury as the concentrations of nerol tested (125 μM to 1 mM) were significantly below the concentrations producing 50% toxicity (IC_{50}) (*SI Appendix*, Fig. S6*D*). These results showing ASM relaxation despite increases in $[Ca^{2+}]_i$ and membrane depolarization suggested an unappreciated functional diversity of Ca^{2+} signaling in the regulation of E-C coupling in ASM.

OR2W3-Evoked Membrane Depolarization Is Linked to SOCE Pathway. To explore the dichotomy of OR2W3-evoked chemosensory responses, we applied pharmacological blockers of Ca^{2+}-selective cation channels that are involved in the E-C coupling mechanisms in smooth muscle (44, 46), as well as potent inhibitors of Ca^{2+}- and cAMP-activated channels that are involved in the induction and adaptation of olfaction (29, 47).

In human ASM cells, treatment with the CNG channel blocker L-cis diltiazem or the adenylyl cyclase inhibitor SQ22536 had little effect on nerol-induced $[Ca^{2+}]_i$ (peak) and ASM relaxation

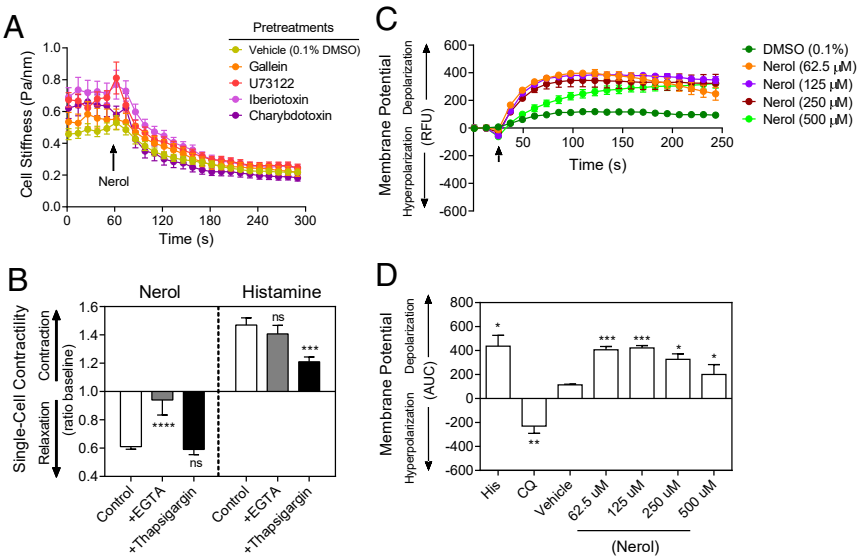

Fig. 6. OR2W3-evoked ASM relaxation is divergent from TAS2R signaling and accompanies membrane depolarization. (*A*) Human ASM cells were treated for 10 min with gallein (20 μM), U73122 (1 μM), iberiotoxin (10 nM), or charybdotoxin (10 nM), and then stimulated with 1 mM nerol. For vehicle control, cells were treated for 10 min with 0.1% DMSO. For each treatment group, baseline stiffness was measured for the first 60 s, and after nerol addition (t = 60 s, arrow), stiffness was continuously measured for the next 240 s. To satisfy the normal distribution assumptions associated with ANOVA, cell stiffness data (steady-state baseline and nerol-induced stiffness) were converted to log scale prior to analyses. Data are presented as mean ± SE (n = 140 to 306 individual cell measurements). (*B*) To chelate extracellular calcium, human ASM cells were treated for 10 min with 2 mM EGTA. To deplete calcium from the intracellular stores, human ASM cells were treated for 20 min with 10 μM thapsigargin (19, 43). ASM cells were then stimulated with 1 mM nerol or 10 μM histamine. Data are presented as mean ± SE (n = 157 to 270 individual cell measurements). We used ANOVA with adjusting for multiple comparisons by applying the Dunnet's method. Treatment groups (EGTA and thapsigargin) were compared with respective Controls for nerol or histamine stimulation. (*C*) Dynamic changes in membrane potential with increasing doses of nerol added at 30 s (arrow) and followed up to 250 s. (*D*) Membrane potential (area under curve, AUC) evoked by nerol in comparison to 10 μM histamine (His) and 1 mM chloroquine (CQ). Data are presented as mean ± SE (n = 3 independent measurements). $*P < 0.05$, $**P < 0.01$, $***P < 0.001$, $****P < 0.0001$ (unpaired t test). ns, not significant.

(*SI Appendix*, Fig. S7*A*). Human ASM cells treated with L-cis diltiazem showed modest increases in $[Ca^{2+}]_i$ (9.6 ± 5.8% from untreated cells) and muscle relaxation (13.8 ± 5.6% from untreated cells) in response to nerol. In addition, nerol-stimulated ASM relaxation was significantly augmented in cells treated with the BK_{Ca} channel inhibitor iberiotoxin (*SI Appendix*, Fig. S7*A*). These results provided a further support that nerol-induced ASM relaxation is not mediated by PKA activity or opening of the BK_{Ca} channels and is independent of Ca^{2+} flux through CNG channels. Of note, we found that pharmacological inhibition of the store-operated calcium channel (SOC) component Orai1 with MRS1845 (48), but not of L-type Ca^{2+} channels with verapamil, inhibited both nerol-evoked increases in $[Ca^{2+}]_i$ and ASM relaxation (*SI Appendix*, Fig. S7*A*). SOC inhibition also markedly attenuated nerol-induced plasma membrane depolarization in human ASM cells (*SI Appendix*, Fig. S7*B*). These data suggest that nerol-evoked Ca^{2+} flux and the associated ASM relaxation involve store-operated calcium entry (SOCE) pathway and membrane depolarization, at the junction between plasma membrane and the ER (49, 50).

Chemosensory Mechanism of OR2W3 Is Tuned to Ca^{2+}-Activated Cl^- Channels. Recently, Li et al. (51) have demonstrated a role for calcium-activated chloride (CaC) channels (Anoctamin 2 [ANO2] or TMEM16B), and the Cl^- current, in chemosensory signal amplification of olfactory transduction in mice. The TMEM16 family of membrane proteins is now considered a bona fide Ca^{2+}-activated Cl^- channel (52–54). Of note, ANO1 (TMEM16A) is broadly expressed (55–59) and, in ASM, TMEM16A expression and activity, but not TMEM16B, modulate smooth muscle tone and shortening (56, 60, 61).

Human ASM cells treated with a pharmacological inhibitor of TMEM16A (100 μM CaCCinh-A01) showed complete reversal of membrane potential in response to nerol (Fig. 7*A*). In addition, consistent with earlier studies using tissues (56, 60, 61), cells treated with CaCCinh-A01 (100 μM) exhibited appreciable decreases in baseline cell stiffness and showed marked decreases in cell stiffening responses to histamine (Fig. 7*B*). Consequently, under these conditions, nerol-induced ASM relaxation was completely ablated (Fig. 7*C*). As this may be attributable to the maximal relaxation of ASM cells caused by TMEM16A inhibition (i.e., no head room left to observe further decreases in stiffness in response to nerol), we lowered the concentration of CaCCinh-A01 (10 μM) pretreatment. Cells treated with 10 μM CaCCinh-A01 exhibited the level of baseline cell stiffness that was comparable to that of untreated cells; and, both showed a similar magnitude of cell stiffening response to histamine (Fig. 7*B*). The subsequent ASM relaxation responses to nerol, however, were markedly attenuated in cells treated with 10 μM CaCCinh-A01 (Fig. 7*C*). These results suggested a close proximity of TMEM16A activation, in time and space, to a macromolecular signaling complex that may be comprised of the assembly of store-operated calcium channel Orai1 and the ER-resident stromal interaction molecule 1 (STIM1) (49, 50). The question then becomes how such signal amplification or electrical responses lead to ASM relaxation.

Using MQAE halide ion-quenched fluorescent indicator, we assessed whether nerol-activated CaC channels cooperatively invoke the electroneutral cation-chloride exchangers (Na^+-K^+-Cl^- cotransporter 1, NKCC1) and the consequent intracellular Cl^- accumulation (56). As a positive control, NaI induced halide into ASM cells in a dose-dependent manner, which was blocked by pretreatment with NPPB, a chloride channel blocker (*SI*

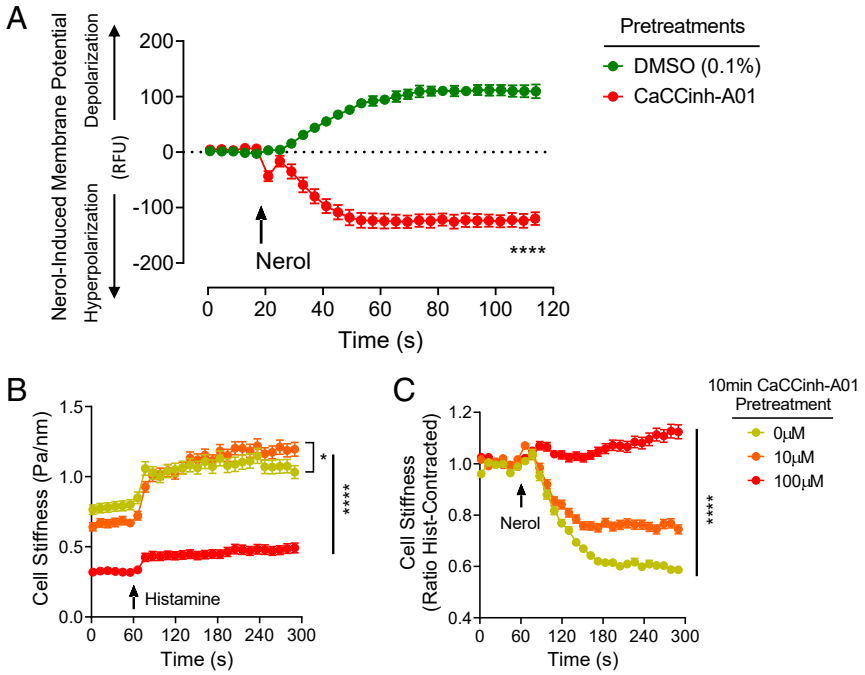

Fig. 7. OR2W3-evoked chemosensory responses are tuned to Ca^{2+}-activated Cl^- channels. (*A*) Nerol-induced changes in membrane potential were measured in cells treated with Ca^{2+}-activated Cl^- (CaC) channel inhibitor (100 μM CaCCinh-A01). For vehicle control, cells were treated with 0.1% DMSO. Arrow indicates time (t = 20 s) at which nerol was added. Data are presented as mean ± SE (n = 3 independent measurements). ****$P < 0.0001$ (area under the curve [AUC], unpaired t test). (*B*) Human ASM cells were treated for 10 min with or without CaCCinh-A01 (10 and 100 μM) and then contracted with 10 μM histamine (histamine was added at t = 60 s, arrow). Data are presented as mean ± SE (n = 228 to 326 cells). ANOVA was applied after data transformation. *$P < 0.05$. (*C*) Histamine-contracted cells were subsequently stimulated with 1 mM nerol. For each individual cell, stiffness was normalized to its stiffness prior to nerol stimulation (nerol was added at t = 60 s, arrow). Data are presented as mean ± SE (n = 182 to 319 individual cell measurements). RFU, relative fluorescence units.

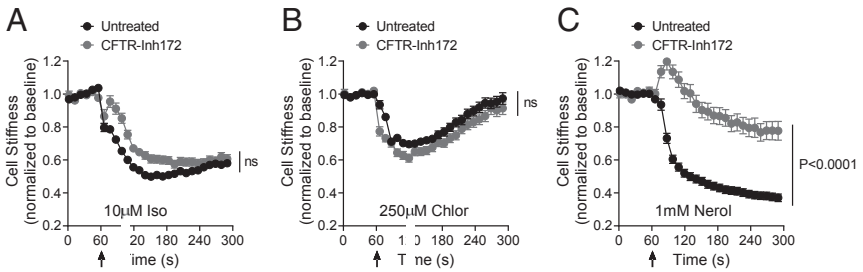

Fig. 8. OR2W3-induced ASM relaxation is inhibited by pharmacological blockers of CFTR. (*A–C*) Human ASM cells were treated with or without 100 μM CFTRinh-172 for 10 min. Using OMTC, we measured the stiffness changes in response to *A* 10 μM isoproterenol, (*B*) 250 μM chloroquine, and (*C*) 1 mM nerol. For each individual cell, stiffness changes were normalized to its respective baseline stiffness. Data are presented as mean ± SE (*A*, $n = 97$ to 168; *B*, $n = 144$ to 145; *C*, $n = 52$ to 185 individual cell measurements).

Appendix, Fig. S7*C*). Nerol had little effect on halide flux in cells treated with or without NPPB; MQAE fluorescent intensities were similar between vehicle (control)- and nerol-stimulated cells (*SI Appendix*, Fig. S7*C*). Moreover, nerol-evoked ASM relaxation was not inhibited by bumetanide, a pharmacological blocker of NKCC1 (*SI Appendix*, Fig. S7*D*), that is involved in the regulation of cell volume and in the accumulation of intracellular Cl^- (62). These results showed that nerol-evoked ASM relaxation is not facilitated by intracellular Cl^- accumulation and/or involves the electroneutral NKCC1 belonging to the SLC12A family of cation-chloride cotransporters.

TMEM16A Cooperates with CFTR to Relax ASM. In differentiated airway epithelial cells, TMEM16A is indispensable for the apical expression of cystic fibrosis transmembrane conductance regulator (CFTR) (63). CFTR is another major secretory anion channel whose defect leads to cystic fibrosis (CF) (64). In human ASM cells, CFTRs are localized to the sarco(endo)plasmic reticulum (65) and are in close proximity to the same microdomains that comprise the assembly of Ca^{2+} and cAMP signaling proteins, including Orai1-STIM1 complex regulating SOCE (49, 50). Most recently, Bozoky et al. (66) reported that CFTR can be directly activated by calcium signaling, independent of PKA phosphorylation. Based on these earlier studies, we considered whether mechanisms of nerol-induced ASM relaxation entail direct activation of CFTR via OR2W3-evoked regulation of $[Ca^{2+}]_i$.

To this end, we treated isolated human ASM cells for 10 min with or without 100 μM of the CFTR inhibitor CFTRinh-172 and subsequently measured dynamic changes in cell stiffness in response to either 10 μM isoproterenol (Fig. 8*A*), 250 μM chloroquine (Fig. 8*B*), or 1 mM nerol (Fig. 8*C*). As shown in Fig. 8, while CFTRinh-172 had little effect on isoproterenol- or chloroquine-induced ASM relaxation, CFTRinh-172 marked attenuated nerol-induced ASM relaxation. On the other hand, nerol-induced ASM relaxation was enhanced in cells treated for 30 min with the CFTR-gating potentiator ivacaftor (*SI Appendix*, Fig. S8*A*). These results established that the mechanism of nerol-induced ASM relaxation is distinct from that of β_2AR and TAS2R pathways, suggesting a role for calcium sequestration through CFTRs expressed on the sarco(endo)plasmic reticulum in human ASM cells. Of note, nerol alone or in combination with ivacaftor (30-min pretreatment) had little effect on the stiffness of human ASM cells derived from a CF lung donor with ΔF508 deletion in CFTR gene (*SI Appendix*, Fig. S8*B*). Taken together, these results are consistent with a mechanistic framework in which nerol-induced ASM relaxation requires cooperative activation of TMEM16A and CFTR to compartmentalize Ca^{2+} signaling within discrete cellular microdomains, including the sequestration of calcium through CFTRs expressed on the endo(sarco)plasmic reticulum of human ASM cells (Fig. 9).

Conclusion

We showed that the monoterpene nerol evokes calcium flux and causes smooth muscle relaxation through OR2W3 expressed on human ASM cells. Paradoxically, we demonstrated that OR2W3-stimulated relaxation of ASM cells requires Ca^{2+} influx and plasma membrane depolarization, and that these chemosensory mechanisms are predominated by a cooperative activation of TMEM16A and CFTR. These observations reveal a previously unrecognized sensory GPCR circuitry in human ASM cells and identify multiple points for signal amplification, attenuation, and duration of chemosensory responses localized to discrete cellular microdomains. Importantly, our study uncovers a surprising role for localized Ca^{2+} regulation that affects E-C coupling mechanisms in human ASM cells.

Methods

Materials. Unless otherwise stated, all odorants of the highest purity available were purchased from Sigma-Aldrich (*SI Appendix*, Table S1). Odorants were freshly prepared on each day of the experiments; they were first reconstituted in DMSO and serially diluted in the appropriate buffer or media. The following pharmacological inhibitors were reconstituted in DMSO, kept at −20 °C, and diluted in the appropriate buffer or media prior to experiments: gallein, U73122, iberiotoxin, charybdotoxin, MRS1845, CaCCinh-A01, H89, CFTRinh-172 (all from Tocris), SQ22536 (Abcam), L-cis diltiazem (Enzo Life Sciences), verapamil (Sigma), and ivacaftor (VX-770, Selleck).

Human ASM Cell Culture. Human ASM cultures were established from the proximal airways (first through third order bronchi) of deceased donor lungs unsuitable for transplantation in accordance with the Institutional Review Boards at Rutgers University. Cells were cultured in Dulbecco's Modified Eagle Medium-Ham's F-12 medium (1:1 vol/vol) supplemented with 10% fetal bovine serum (FBS), antibiotics (100 U/mL penicillin, 100 μg/mL streptomycine), and 2.5 μg/mL amphotericin-β. As described elsewhere (7), cells were grown until confluence at 37 °C in humidified air containing 5% CO_2 and then maintained in serum-free media for at least 24 h prior to all experiments. In this study, cells were used at or before passage 6.

Generation of PCLS and Bronchodilation Assays. hPCLSs were prepared as previously described (67, 68). In brief, whole human lungs from three non-asthmatic donors were dissected and inflated using 2% (wt/vol) low melting point agarose. Once the agarose set, the lobe was section, and cores of 8-mm diameter were made. The cores that contained a small airway by visual inspection were sliced at a thickness of 350 μm (Precisionary Instruments VF300 Vibratome) and collected in wells containing supplemented Ham's F-12 medium. Suitable airways (≤1-mm diameter) on slices were selected on the basis of the following criteria: presence of a full smooth muscle wall, presence of beating cilia, and unshared muscle walls at airway branch points to eliminate possible counteracting contractile forces. Each slice contained ~98% parenchyma tissue; hence, all airways situated on a slice had sufficient parenchymal tissue to impart basal tone. Adjacent slices containing contiguous segments of the same airway were paired and served as controls and were incubated at 37 °C in a humidified air-CO_2 (95 to 5%) incubator. Sections were rinsed with fresh media two to three times on day 1 and day 2 to remove agarose and endogenous substances released that variably

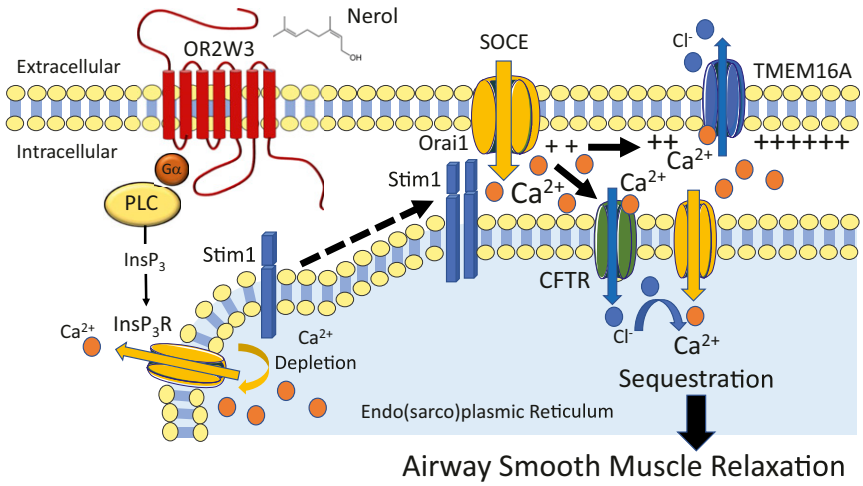

Fig. 9. Conceptual model of OR2W3-evoked ASM relaxation and bronchodilation. Activation of the odorant receptor OR2W3, a GPCR expressed on human ASM cells causes Ca^{2+} release through PLCβ-IP3 signaling leading to decline in Ca^{2+} in the intracellular store [endo(sarco)plasmic reticulum, ER/SR]. The reduction in ER Ca^{2+} initiates extracellular calcium influx through the SOCE pathway via activation of Stim1 and its subsequent physical interactions with Orai1 at the discrete cellular microdomains. Ca^{2+} flux through store-operated calcium channels leads to plasma membrane depolarization and is potentiated by a cooperative activation of TMEM16A and CFTR localized at the same junction between plasma membrane and the ER/SR. The action of the latter causes Cl^- uptake into the SR, facilitating Ca^{2+} sequestration that results in a decrease in cytosolic calcium concentration promoting ASM relaxation.

confound the production of inflammatory mediators and/or alter airway tone (67, 68). Airways were bronchoconstricted to carbachol (10^{-5} M), followed by sequential stimulation with increasing doses of nerol (250 μM, 500 μM, 1 mM, and 3 mM) and then forskolin (10^{-5} M).

To assess luminal area, lung slices were placed in a 12-well plate in media and held in place using a nylon weight with platinum attachments. The airway was located using a microscope (Nikon Eclipse; model no. TE2000-U; magnification, ×40) connected to a live video feed (Evolution QEi; model no. 32-0074A-130 video recorder). Airway luminal area was measured using Image-Pro Plus software (version 6.0; Media Cybernetics) and represented in units of square micrometers (67, 68). Bronchodilation was calculated as the percent reversal of maximal bronchoconstriction.

Quantitative Reverse Transcription PCR (qRT-PCR). RNA was extracted from human ASM cells using the RNeasy Mini Kit (Qiagen) and digested with RNase-free DNase (Qiagen) according to the manufacturer's protocol. RNA was reverse transcribed using the High-Capacity cDNA Reverse Transcription Kit (Applied Biosystems, Fisher Scientific), and no-enzyme controls (in which the reverse transcriptase was replaced with water) were made concurrently. Real-time PCR was performed using TaqMan probes for OR2W3 or SYBR green primers for OR2W3 (forward: 5′ CTGCCGGGGCTTGGTGTCAG 3′, reverse: 5′ TCCACCTCGTGGTGCCCACA 3′) using a StepOne real-time PCR system (Thermo Fisher).

PCR. PCR was performed with TaKaRa Taq DNA Polymerase (Clontech) at an annealing temperature of 50 °C to amplify the full-length OR2W3. To verify the product size, PCR products were visualized by UV after ethidium bromide staining on agarose gels.

Immunocytochemistry. Human ASM cells were seeded on 12-mm glass coverslips (VWR) at 30,000 cells/coverslip. The adherent cells were fixed with 4% paraformaldehyde in phosphate-buffered saline (PBS) for 20 min, washed three times in PBS, and permeabilized with 0.2% Triton X-100 (Bio-Rad) for 15 min at room temperature. Coverslips were then blocked with 2% bovine serum albumin (BSA) in PBS for 1 h at room temperature and incubated overnight at 4 °C with mouse anti-OR2W3 primary antibody (1:300, Sigma). Subsequently, coverslips were incubated with an Alexa Fluor goat anti-mouse 488 (1:400, The Jackson Laboratory) for 1 h at room temperature. Coverslips were washed three times with 2% BSA in PBS and mounted with ProLong Gold Antifade Mountant with DAPI (Thermo Fisher). Samples were imaged at 20× magnification.

The sensitivity of the OR2W3 antibody (Sigma) was tested by transfecting HEK 293T cells with Flag-tagged OR2W3 or Flag-tagged Olfr78, as we have previously done for OR trafficking and surface localization studies (17, 69, 70). This consisted of first staining live nonpermeabilized cells with rabbit polyclonal anti-Flag antibody (Sigma) at 4 °C. Cells were then fixed, permeabilized, and stained with mouse anti-OR2W3 primary antibody (1:300, Sigma). Primary antibodies were detected using Alexa Fluor goat anti-rabbit 555 (for surface OR) and goat anti-mouse 488 (for internal OR) secondary antibodies, and nucleus was stained with Hoechst 33342 (1:2,500).

Western Blotting. Cells were grown in six-well plates to confluency, followed by 24-h serum deprivation. Serum-deprived cells were washed with PBS and lysed with 1× SDS Protein Gel Loading Solution (Quality Biological, Inc.). Proteins were separated by SDS/PAGE and transferred to nitrocellulose membranes. Membranes were blocked with 5% BSA in Tris-buffered saline with 0.1% Tween 20, and incubated with primary antibodies overnight (OR2W3 [1:1,000; GeneTex] and tubulin [1:500; Sigma]), followed by HRP-conjugated secondary antibody for 1 h. HRP-labeled bands were detected using an enhanced chemiluminescence (ECL) kit (Pierce) according to the manufacturer's instructions. The specificity of the OR2W3 antibody (GeneTex) was verified by blocking peptide competition assay.

Calcium Imaging. Intracellular calcium ($[Ca^{2+}]_i$) for the initial odor screen was quantified using the FLIPR Calcium 5 assay kit (Molecular Devices). Human ASM cells were seeded at 30,000 cells/well in collagen I-coated wells (96-well black-well/clear-bottom plates, Corning) in serum-free media. Cells were incubated with Calcium 5 dye for 1 h at 37 °C and subsequently allowed to recover at room temperature for 15 min. Odorants were added, and fluorescent readings were measured using a FlexStation 3 (Molecular Devices). Hanks' balanced salt solution (HBSS) adjusted to a pH of 7.4 and supplemented with 20 mM Hepes was used during the experiments and as a buffer to dilute the Calcium 5 dye.

For $[Ca^{2+}]_i$ imaging in individual cells, ratiometric calcium indicator Fura-2 was used under the same experimental condition as FLIPR calcium imaging. In brief, cells were incubated with 2 μM Fura-2 for 45 min, washed three times with buffer, and incubated for another 30 min without Fura-2 prior to imaging. Cells were imaged sequentially at 340 nm and 380 nm, and 30 to 45 cells per field of view were used to calculate the 340/380 ratio. The buffer used to dilute Fura-2 and during the course of the experiment was HBSS supplemented with 10 mM Hepes, 11 mM glucose, 2.5 mM $CaCl_2$, and 1.2 mM $MgCl_2$ (pH adjusted to 7.4). Calcium-free medium was similarly made, with the exclusion of $CaCl_2$.

cAMP Assay. Primary human ASM cells seeded in six-well plates were incubated in lysis buffer for 20 min at 4 °C and dissociated using cell scrapers. Cell samples were subsequently centrifuged at 16,100 rcf for 10 min, and supernatants were collected. Protein concentrations were measured using a Pierce BCA protein assay kit (Thermo Scientific). Diluted samples and cAMP standards were acetylated for increased sensitivity, and cAMP concentrations were measured using a colorimetric cAMP ELISA kit (Cell Biolabs) according to the manufacturer's protocol.

OMTC. Dynamic changes in cell stiffness were measured as an indicator of the single-cell contraction and/or relaxation of isolated human ASM cells as we have previously described (7). In brief, RGD-coated ferrimagnetic microbeads (4.5 μm in diameter) bound to the cytoskeleton through cell surface integrin receptors were magnetized horizontally and then twisted in a vertically aligned homogeneous magnetic field that was varying sinusoidally in time. This sinusoidal twisting magnetic field caused both a rotation and a pivoting displacement of the bead: as the bead moves, the cell develops internal stresses which in turn resist bead motions (71). Lateral bead displacements in response to the resulting oscillatory torque were detected with a spatial resolution of ~5 nm, and the ratio of specific torque to bead displacements was computed and expressed here as the cell stiffness in units of Pascal per nanometer (Pa/nm).

Short Hairpin RNA-Mediated OR2W3 Silencing. Bacterial glycerol stocks of two precloned short hairpin RNAs (shRNAs), each targeting a different region of the human *OR2W3* gene, were obtained from the Sigma TRC 1.5 shRNA library (TRCN0000204524 and TRCN0000187944 from The RNAi Consortium, Sigma). A control shRNA that has the same pLKO.1 plasmid was also used. Bacteria from glycerol stocks were streaked onto an LB agar plate and grown overnight at 37 °C. A single colony from each plate was inoculated in liquid LB with ampicillin (100 μg/mL), and plasmid DNA was isolated using the QIAGEN Plasmid Midi Kit (Qiagen) per manufacturer's protocol. To produce lentivirus, the plasmid DNA was cotransfected into HEK 293T cells with packaging plasmids pMD2.G and psPAX2 (Addgene) using the calcium phosphate transfection method in 100 mm cell culture dishes. Lentivirus was harvested 48 h after transfection and filtered through a 0.45-μm cellulose acetate filter (Sigma). The packaged lentivirus was then transduced into ASM cells using T25 flasks, followed by puromycin selection for 2 to 3 d. The surviving cells were used for subsequent experiments to test knockdown efficiency and cell function.

Membrane Potential. Changes in membrane potential were measured using the FLIPR Membrane Potential Assay Kit Blue (Molecular Devices). In brief, human ASM cells seeded at 40,000 cells/well in 96-well plates were incubated with dye in HBSS supplemented with 20 mM Hepes for 10 min at 25 °C in the dark. Fluorescence signals were measured using a FlexStation 3 (Molecular Devices), with baseline fluorescence (excitation 530 nm, emission 565 nm, cutoff 550 nm) measurements taken for 16 s before addition of agonists. Signals were acquired every 2 s for a total of 2 min. An increase or decrease in fluorescence after cell stimulation indicates cell membrane depolarization or hyperpolarization, respectively.

LDH Toxicity Assay. Primary human ASM cells adherent on 96-well plates were incubated with 125 to 3,000 μM nerol for 1 h and 24 h, and the release of lactose dehydrogenase (LDH) was measured using the Pierce LDH Cytotoxicity Assay Kit (Thermo Fisher) according to the manufacturer's protocols.

Halide Flux Measurement. Primary human ASM cells were seeded at 10,000 cells/well in collagen I-coated 96-well, black-well plates, and cultured overnight. The next day, cells were incubated with 10 mM MQAE (Invitrogen) in serum-free media for 10 h at 37 °C. Cells were washed three times with physiological buffer solution (10 mM Hepes pH 7.4, 10 mM glucose, 2.4 mM K_2PO_4, 0.6 mM K_2HPO_4, 1 mM $MgSO_4$, 1 mM $CaSO_4$, and 110 mM sodium isethionate) and were subsequently loaded with either 100 μM chloride channel blocker or 0.1% DMSO vehicle in 100 μL physiological buffer for 30 min. Changes in the fluorescence intensity of MQAE indicator quenched by halide ion was measured with a FlexStation 3 device (Molecular Devices). Baseline fluorescence (excitation 360 nm, emission 460 nm, cutoff 455 nm) measurements were taken every 2 s for a total of 2 min, and after addition of either nerol or NaI (as a positive control), changes in the fluorescence were continuously recorded for an additional 3 min. A decline in fluorescence after adding agonists indicates accumulation of halide ions inside the cells.

Data Analysis. Unless otherwise stated, data are presented as mean ± SEM. Statistical comparisons were done with two-tailed, unpaired Student's *t* tests, as well as the analysis of variance (ANOVA) with adjusting for multiple comparisons by applying the Dunnett's method. Analyses were performed using GraphPad Prism, and two-sided *P* values less than 0.05 were considered significant.

Data Availability. All study data are included in the article and supporting information.

ACKNOWLEDGMENTS. This work was supported by the New Jersey Alliance for Clinical and Translational Science (UL1TR0030117) and the National Institutes of Health grants: P01HL114471 (to S.S.A., R.B.P., S.B.L., and R.A.P.), R01HL137030 (to D.A.D.), R01HL058506 (to R.B.P.), R01NS054791 (to X.D), and R01AI135186 (to X.D.). X.D. is an investigator of the Howard Hughes Medical Institute. S.S.A. was also supported by a Discovery Award and a Catalyst Award from Johns Hopkins University, the Patrick C. Walsh Prostate Cancer Research Fund from the James Buchanan Brady Urological Institute (The Frank E. Rath Spang & Company Charitable Trust Scholar), and Maryland Cigarette Restitution Fund from the State of Maryland Department of Health and Mental Hygiene.

1. M. Masoli, D. Fabian, S. Holt, R. Beasley; Global Initiative for Asthma (GINA) Program, The global burden of asthma: Executive summary of the GINA dissemination committee report. *Allergy* **59**, 469–478 (2004).
2. P. J. Sterk, E. H. Bel, Bronchial hyperresponsiveness: The need for a distinction between hypersensitivity and excessive airway narrowing. *Eur. Respir. J.* **2**, 267–274 (1989).
3. A. J. Woolcock, J. K. Peat, Epidemiology of bronchial hyperresponsiveness. *Clin. Rev. Allergy* **7**, 245–256 (1989).
4. S. S. An *et al*., Airway smooth muscle dynamics: A common pathway of airway obstruction in asthma. *Eur. Respir. J.* **29**, 834–860 (2007).
5. J. L. Black, P. R. Johnson, Airway smooth muscle in asthma. *Respirology* **1**, 153–158 (1996).
6. G. G. King, P. D. Paré, C. Y. Seow, The mechanics of exaggerated airway narrowing in asthma: The role of smooth muscle. *Respir. Physiol.* **118**, 1–13 (1999).
7. S. S. An *et al*., An inflammation-independent contraction mechanophenotype of airway smooth muscle in asthma. *J. Allergy Clin. Immunol.* **138**, 294–297.e4 (2016).
8. O. Kilic *et al*., A microphysiological model of the bronchial airways reveals the interplay of mechanical and biochemical signals in bronchospasm. *Nat. Biomed. Eng.* **3**, 532–544 (2019).
9. P. J. Barnes, New drugs for asthma. *Nat. Rev. Drug Discov.* **3**, 831–844 (2004).
10. S. J. Morgan *et al*., β-Agonist-mediated relaxation of airway smooth muscle is protein kinase A-dependent. *J. Biol. Chem.* **289**, 23065–23074 (2014).
11. M. R. Sears *et al*., Regular inhaled beta-agonist treatment in bronchial asthma. *Lancet* **336**, 1391–1396 (1990).
12. H. S. Nelson, S. T. Weiss, E. R. Bleecker, S. W. Yancey, P. M. Dorinsky; SMART Study Group, The salmeterol multicenter asthma research trial: A comparison of usual pharmacotherapy for asthma or usual pharmacotherapy plus salmeterol. *Chest* **129**, 15–26 (2006).
13. D. Cheung *et al*., Long-term effects of a long-acting beta 2-adrenoceptor agonist, salmeterol, on airway hyperresponsiveness in patients with mild asthma. *N. Engl. J. Med.* **327**, 1198–1203 (1992).
14. J. Kraan, G. H. Koëter, T. W. vd Mark, H. J. Sluiter, K. de Vries, Changes in bronchial hyperreactivity induced by 4 weeks of treatment with antiasthmatic drugs in patients with allergic asthma: A comparison between budesonide and terbutaline. *J. Allergy Clin. Immunol.* **76**, 628–636 (1985).
15. R. Beasley, N. Pearce, J. Crane, C. Burgess, Beta-agonists: What is the evidence that their use increases the risk of asthma morbidity and mortality? *J. Allergy Clin. Immunol.* **104**, S18–S30 (1999).
16. S. R. Salpeter, A. J. Wall, N. S. Buckley, Long-acting beta-agonists with and without inhaled corticosteroids and catastrophic asthma events. *Am. J. Med.* **123**, 322–8.e2 (2010).
17. W. H. Aisenberg *et al*., Defining an olfactory receptor function in airway smooth muscle cells. *Sci. Rep.* **6**, 38231 (2016).
18. S. S. An, S. B. Liggett, Taste and smell GPCRs in the lung: Evidence for a previously unrecognized widespread chemosensory system. *Cell. Signal.* **41**, 82–88 (2018).
19. D. A. Deshpande *et al*., Bitter taste receptors on airway smooth muscle bronchodilate by localized calcium signaling and reverse obstruction. *Nat. Med.* **16**, 1299–1304 (2010).
20. S. S. An, K. S. Robinett, D. A. Deshpande, W. C. Wang, S. B. Liggett, Reply to: Activation of BK channels may not be required for bitter tastant-induced bronchodilation. *Nat. Med.* **18**, 650–651 (2012).
21. S. S. An *et al*., TAS2R activation promotes airway smooth muscle relaxation despite β(2)-adrenergic receptor tachyphylaxis. *Am. J. Physiol. Lung Cell. Mol. Physiol.* **303**, L304–L311 (2012).
22. D. A. Deshpande *et al*., Bronchodilator activity of bitter tastants in human tissue. *Nat. Med.* **17**, 776–778 (2011).
23. S. J. Lee, I. Depoortere, H. Hatt, Therapeutic potential of ectopic olfactory and taste receptors. *Nat. Rev. Drug Discov.* **18**, 116–138 (2019).
24. M. Parmentier *et al*., Expression of members of the putative olfactory receptor gene family in mammalian germ cells. *Nature* **355**, 453–455 (1992).
25. M. Spehr *et al*., Identification of a testicular odorant receptor mediating human sperm chemotaxis. *Science* **299**, 2054–2058 (2003).
26. C. Flegel *et al*., Characterization of the olfactory receptors expressed in human spermatozoa. *Front. Mol. Biosci.* **2**, 73 (2016).
27. L. Buck, R. Axel, A novel multigene family may encode odorant receptors: A molecular basis for odor recognition. *Cell* **65**, 175–187 (1991).
28. J. Bradley, J. Li, N. Davidson, H. A. Lester, K. Zinn, Heteromeric olfactory cyclic nucleotide-gated channels: A subunit that confers increased sensitivity to cAMP. *Proc. Natl. Acad. Sci. U.S.A.* **91**, 8890–8894 (1994).
29. S. D. Munger, Olfaction: Noses within noses. *Nature* **459**, 521–522 (2009).

30. S. Katada, T. Hirokawa, Y. Oka, M. Suwa, K. Touhara, Structural basis for a broad but selective ligand spectrum of a mouse olfactory receptor: Mapping the odorant-binding site. *J. Neurosci.* **25**, 1806–1815 (2005).
31. H. Kida *et al*., Vapor detection and discrimination with a panel of odorant receptors. *Nat. Commun.* **9**, 4556 (2018).
32. K. Schmiedeberg *et al*., Structural determinants of odorant recognition by the human olfactory receptors OR1A1 and OR1A2. *J. Struct. Biol.* **159**, 400–412 (2007).
33. M. D. Bhaskaran, B. N. Smith, Cannabinoid-mediated inhibition of recurrent excitatory circuitry in the dentate gyrus in a mouse model of temporal lobe epilepsy. *PLoS One* **5**, e10683 (2010).
34. K. Jiang *et al*., Geraniol alleviates LPS-induced acute lung injury in mice via inhibiting inflammation and apoptosis. *Oncotarget* **8**, 71038–71053 (2017).
35. A. Kozioł *et al*., An overview of the pharmacological properties and potential applications of natural monoterpenes. *Mini Rev. Med. Chem.* **14**, 1156–1168 (2014).
36. N. Yadav, H. Chandra, Suppression of inflammatory and infection responses in lung macrophages by eucalyptus oil and its constituent 1,8-cineole: Role of pattern recognition receptors TREM-1 and NLRP3, the MAP kinase regulator MKP-1, and NFκB. *PLoS One* **12**, e0188232 (2017).
37. S. J. Mundell, M. E. Olah, R. A. Panettieri, J. L. Benovic, R. B. Penn, Regulation of G protein-coupled receptor-adenylyl cyclase responsiveness in human airway smooth muscle by exogenous and autocrine adenosine. *Am. J. Respir. Cell Mol. Biol.* **24**, 155–163 (2001).
38. G. Ortar *et al*., Effect of acyclic monoterpene alcohols and their derivatives on TRP channels. *Bioorg. Med. Chem. Lett.* **24**, 5507–5511 (2014).
39. M. J. Pérez de Vega, I. Gómez-Monterrey, A. Ferrer-Montiel, R. González-Muñiz, Transient receptor potential melastatin 8 channel (TRPM8) modulation: Cool entryway for treating pain and cancer. *J. Med. Chem.* **59**, 10006–10029 (2016).
40. S. C. Stotz, J. Vriens, D. Martyn, J. Clardy, D. E. Clapham, Citral sensing by transient [corrected] receptor potential channels in dorsal root ganglion neurons. *PLoS One* **3**, e2082 (2008).
41. Y. Jiang *et al*., Molecular profiling of activated olfactory neurons identifies odorant receptors for odors in vivo. *Nat. Neurosci.* **18**, 1446–1454 (2015).
42. B. von der Weid *et al*., Large-scale transcriptional profiling of chemosensory neurons identifies receptor-ligand pairs in vivo. *Nat. Neurosci.* **18**, 1455–1463 (2015).
43. S. S. An, C. M. Hai, Mechanical signals and mechanosensitive modulation of intracellular [Ca(2+)] in smooth muscle. *Am. J. Physiol. Cell Physiol.* **279**, C1375–C1384 (2000).
44. A. P. Somlyo, A. V. Somlyo, Signal transduction and regulation in smooth muscle. *Nature* **372**, 231–236 (1994).
45. T. Pera, R. B. Penn, Bronchoprotection and bronchorelaxation in asthma: New targets, and new ways to target the old ones. *Pharmacol. Ther.* **164**, 82–96 (2016).
46. M. Schramm, G. Thomas, R. Towart, G. Franckowiak, Novel dihydropyridines with positive inotropic action through activation of Ca2+ channels. *Nature* **303**, 535–537 (1983).
47. D. Schild, D. Restrepo, Transduction mechanisms in vertebrate olfactory receptor cells. *Physiol. Rev.* **78**, 429–466 (1998).
48. K. Ma *et al*., Phosphate-induced ORAI1 expression and store-operated Ca^{2+} entry in aortic smooth muscle cells. *J. Mol. Med. (Berl.)* **97**, 1465–1475 (2019).
49. X. Cao *et al*., The ER/PM microdomain, $PI(4,5)P_2$ and the regulation of STIM1-Orai1 channel function. *Cell Calcium* **58**, 342–348 (2015).
50. A. Son, S. Park, D. M. Shin, S. Muallem, Orai1 and STIM1 in ER/PM junctions: Roles in pancreatic cell function and dysfunction. *Am. J. Physiol. Cell Physiol.* **310**, C414–C422 (2016).
51. R. C. Li *et al*., Ca^{2+}-activated Cl current predominates in threshold response of mouse olfactory receptor neurons. *Proc. Natl. Acad. Sci. U.S.A.* **115**, 5570–5575 (2018).
52. A. Caputo *et al*., TMEM16A, a membrane protein associated with calcium-dependent chloride channel activity. *Science* **322**, 590–594 (2008).
53. B. C. Schroeder, T. Cheng, Y. N. Jan, L. Y. Jan, Expression cloning of TMEM16A as a calcium-activated chloride channel subunit. *Cell* **134**, 1019–1029 (2008).
54. Y. D. Yang *et al*., TMEM16A confers receptor-activated calcium-dependent chloride conductance. *Nature* **455**, 1210–1215 (2008).
55. F. Huang *et al*., Studies on expression and function of the TMEM16A calcium-activated chloride channel. *Proc. Natl. Acad. Sci. U.S.A.* **106**, 21413–21418 (2009).
56. G. Gallos *et al*., Functional expression of the TMEM16 family of calcium-activated chloride channels in airway smooth muscle. *Am. J. Physiol. Lung Cell. Mol. Physiol.* **305**, L625–L634 (2013).
57. U. Oh, J. Jung, Cellular functions of TMEM16/anoctamin. *Pflugers Arch.* **468**, 443–453 (2016).
58. N. Pedemonte, L. J. Galietta, Structure and function of TMEM16 proteins (anoctamins). *Physiol. Rev.* **94**, 419–459 (2014).
59. C. Flegel *et al*., RNA-seq analysis of human trigeminal and dorsal root ganglia with a focus on chemoreceptors. *PLoS One* **10**, e0128951 (2015).
60. J. Danielsson *et al*., Agonism of the TMEM16A calcium-activated chloride channel modulates airway smooth muscle tone. *Am. J. Physiol. Lung Cell. Mol. Physiol.* **318**, L287–L295 (2020).
61. J. Danielsson *et al*., Antagonists of the TMEM16A calcium-activated chloride channel modulate airway smooth muscle tone and intracellular calcium. *Anesthesiology* **123**, 569–581 (2015).
62. T. Garzon-Muvdi *et al*., Regulation of brain tumor dispersal by NKCC1 through a novel role in focal adhesion regulation. *PLoS Biol.* **10**, e1001320 (2012).
63. R. Benedetto *et al*., Epithelial chloride transport by CFTR requires TMEM16A. *Sci. Rep.* **7**, 12397 (2017).
64. G. R. Cutting, Cystic fibrosis genetics: From molecular understanding to clinical application. *Nat. Rev. Genet.* **16**, 45–56 (2015).
65. D. P. Cook *et al*., Cystic fibrosis transmembrane conductance regulator in sarcoplasmic reticulum of airway smooth muscle. Implications for airway contractility. *Am. J. Respir. Crit. Care Med.* **193**, 417–426 (2016).
66. Z. Bozoky *et al*., Synergy of cAMP and calcium signaling pathways in CFTR regulation. *Proc. Natl. Acad. Sci. U.S.A.* **114**, E2086–E2095 (2017).
67. P. R. Cooper *et al*., TLR3 activation stimulates cytokine secretion without altering agonist-induced human small airway contraction or relaxation. *Am. J. Physiol. Lung Cell. Mol. Physiol.* **297**, L530–L537 (2009).
68. C. J. Koziol-White *et al*., Inhibition of spleen tyrosine kinase attenuates IgE-mediated airway contraction and mediator release in human precision cut lung slices. *Br. J. Pharmacol.* **173**, 3080–3087 (2016).
69. J. L. Pluznick *et al*., Olfactory receptor responding to gut microbiota-derived signals plays a role in renin secretion and blood pressure regulation. *Proc. Natl. Acad. Sci. U.S.A.* **110**, 4410–4415 (2013).
70. B. D. Shepard, N. Natarajan, R. J. Protzko, O. W. Acres, J. L. Pluznick, A cleavable N-terminal signal peptide promotes widespread olfactory receptor surface expression in HEK293T cells. *PLoS One* **8**, e68758 (2013).
71. B. Fabry *et al*., Scaling the microrheology of living cells. *Phys. Rev. Lett.* **87**, 148102 (2001).